

# Analytical Model of Nonlinear, Single-Mode, Classical Rayleigh–Taylor Instability at Arbitrary Atwood Numbers

An interface between two fluids subject to an external force pointing from the heavier to the lighter fluid is hydrodynamically unstable<sup>1</sup> [Rayleigh–Taylor (RT) instability]. This instability plays an important role in astrophysics and inertial confinement fusion.<sup>2</sup> In the limit of small perturbation amplitudes  $\eta$  ( $k\eta \ll 1$ , where  $k$  is the perturbation wave number), the perturbations grow exponentially<sup>1</sup>  $\eta \sim \eta_0 e^{\gamma t}$  with the growth rate  $\gamma = \sqrt{A_T k g}$ , where  $A_T = (\rho_h - \rho_l)/(\rho_h + \rho_l)$  is the Atwood number,  $\rho_h$  and  $\rho_l$  are the densities of heavier and lighter fluids, respectively,  $g$  is the interface acceleration, and  $\eta_0$  is the initial amplitude. As the amplitude becomes large enough ( $k\eta \sim 1$ ), the interface can be divided into the spikes of the heavier fluid penetrating into the lighter fluid and bubbles of the lighter fluid rising into the heavier fluid. The exponential growth of the bubble amplitude changes to the linear-in-time growth<sup>3–8</sup>  $\eta \sim U_b t$ , where  $U_b$  is the bubble velocity. Such a transition is commonly referred to as a “nonlinear saturation,” although, strictly speaking, only the bubble velocity saturates, not the amplitude. To describe the evolution of the perturbation after the saturation, two analytical approaches have been proposed in the past.<sup>3–8</sup> The weakly nonlinear theories<sup>5</sup> (up to the third-order accuracy in  $k\eta$ ) capture only the initial slowing down of the exponential growth. The other approach uses an expansion of the perturbation amplitudes and conservation equations near the tip of the bubble<sup>3,4,7,8</sup> (or spike<sup>8</sup>) up to the second or higher order in the transverse coordinate. In the past, the second approach has been applied only to the fluid–vacuum interfaces ( $A_T = 1$ )<sup>3,4,6–8</sup> and has been shown to be in good agreement with numerical simulations and experimental data. In this article, the Layzer’s theory will be extended to include finite density of the lighter fluid ( $A_T \leq 1$ ). We also report an exact solution of conservation equations (valid at the tip of the bubble) in the form of a convergent Fourier series.

First, we consider two irrotational, incompressible, inviscid fluids in two-dimensional (2-D) geometry. The fluids are subject to an external acceleration  $g$  pointing from the heavier to the lighter fluid. The  $y$  axis is chosen in the direction of the density gradient. The velocity potential  $\phi$  in the absence of viscosity and thermal conduction obeys the Laplace equation

$$\Delta\phi = \partial_x^2\phi + \partial_y^2\phi = 0. \quad (1)$$

In addition, the function  $\phi$  must satisfy the following jump conditions at the fluid interface  $y = \eta(x, t)$ :

$$\partial_t\eta + \mathbf{v}_x^h \partial_x \eta = \mathbf{v}_y^h, \quad (2)$$

$$\left[ \left[ \mathbf{v}_y - \mathbf{v}_x \partial_x \eta \right] \right] = 0, \quad (3)$$

$$\left[ \left[ \rho \left( \partial_t \phi + \frac{1}{2} \mathbf{v}^2 + g\eta \right) \right] \right] = f(t), \quad (4)$$

where  $\left[ \left[ Q \right] \right] = Q^h = Q^l$  (superscripts  $h$  and  $l$  denote the heavy- and light-fluid variables, respectively) and  $f(t)$  is an arbitrary function of time. Equations (2) and (3) are derived from the mass-conservation equation and continuity condition for the velocity component normal to the fluid interface, and Eq. (4) is the Bernoulli’s equation. Following Ref. 4, we expand Eqs. (2)–(4) and the interface amplitude  $\eta$  near the tip of the bubble [localized at the point  $\{x, y\} = \{0, \eta(0, t)\}$ ] to the second order in  $x$ ,  $\eta = \eta_0(t) + \eta_2(t)x^2$ . The function  $\eta_2(t)$  is related to the bubble curvature  $R$  as  $R = -1/(2\eta_2)$ . To satisfy boundary conditions (2)–(4) (six equations), we need six unknowns. Thus, in addition to the functions  $\eta_0(t)$ ,  $\eta_2(t)$ , and  $f(t)$ , the velocity potential must contain three unknowns. We write the velocity potential near the bubble tip in the following form:

$$\phi^h = a_1(t) \cos(kx) e^{-k(y-\eta_0)}, \quad (5)$$

$$\phi^l = b_1(t) \cos(kx) e^{k(y-\eta_0)} + b_2(t)y. \quad (6)$$

The form of the light-fluid potential [Eq. (6)] will be verified later using the results of numerical simulations. Substituting Eqs. (5) and (6) into the boundary conditions (2)–(4) and

expanding the latter near the bubble tip gives

$$\dot{\eta}_2 = -\dot{\eta}_0 \frac{k}{2}(k + 6\eta_2), \quad (7)$$

$$\begin{aligned} & \ddot{\eta}_0 \frac{k^2 - 4A_T k \eta_2 - 12A_T \eta_2^2}{2(k - 6\eta_2)} \\ & + \dot{\eta}_0^2 k^2 \frac{(4A_T - 3)k^2 + 6(3A_T - 5)k\eta_2 + 36A_T \eta_2^2}{2(k - 6\eta_2)^2} \\ & + A_T g \eta_2 = 0. \end{aligned} \quad (8)$$

Equation (7) can be integrated directly. The result, assuming initial sinusoidal perturbation with amplitude  $\eta_0(0)$ , takes the form

$$\eta_2 = -\frac{k}{6} + \left[ \frac{k}{6} - \eta_0(0) \frac{k^2}{2} \right] e^{-3k[\eta_0 - \eta_0(0)]}. \quad (9)$$

Furthermore, substituting Eq. (9) into Eq. (8), the latter can be integrated to give an analytic expression for the bubble velocity. This expression is very lengthy, however, and will be reported elsewhere. In practice, one can easily calculate the bubble amplitude by solving the system (7)–(8) using, for example, the *Mathematica* software package.<sup>9</sup> Next, we obtained an asymptotic solution for the bubble velocity by taking the limit of  $t \rightarrow \infty$  in Eqs. (9) and (8). This gives

$$\eta_2 \rightarrow -\frac{k}{6}, \quad U_b \rightarrow \sqrt{\frac{2A_T}{1+A_T} \frac{g}{3k}}. \quad (10)$$

The last equation agrees with the prediction of the drag–buoyancy model.<sup>6</sup> Solution of Eq. (8) provides a continuous bubble evolution from the linear to the nonlinear regime, while the drag–buoyancy model calculates only the asymptotic behavior.

Next, we verify the choice of the velocity potential in the light fluid [Eq. (6)] by comparing the velocity profiles obtained from Eq. (6) and full numerical simulation. For such purpose, we first calculate the coefficients  $b_1$  and  $b_2$  as functions of time:

$$b_1 = \dot{\eta}_0 \frac{6\eta_2 + k}{k(k - 6\eta_2)}, \quad b_2 = \frac{12\dot{\eta}_0 \eta_2}{6\eta_2 - k}. \quad (11)$$

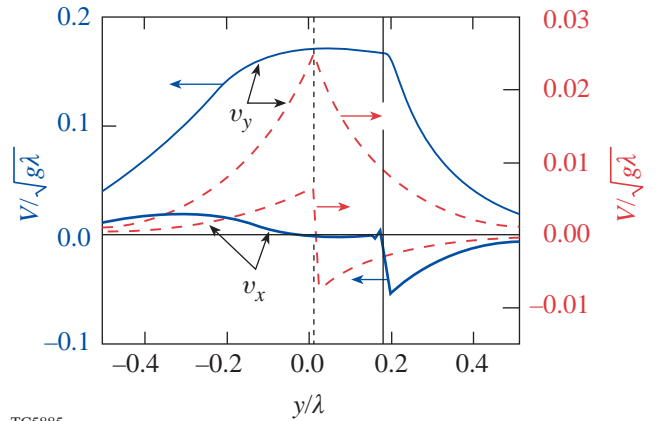
Since  $\eta_2(t \rightarrow \infty) = -k/6$ , then  $b_1 \rightarrow 0$  and  $b_2 \rightarrow \dot{\eta}_0$ . Then, substituting Eq. (11) into the definition of the light-fluid velocity,

$$v_x^l = -b_1 k \sin(kx) e^{k(y - \eta_0)}$$

and

$$v_y^l = b_1 k \cos(kx) e^{k(y - \eta_0)} + b_2,$$

we find that asymptotically, the light-fluid velocity component parallel to the acceleration becomes flat near the tip of the bubble (no  $x$  or  $y$  dependence), and the transverse velocity component in that region goes to zero. To confirm this result, we performed a 2-D simulation using an incompressible, inviscid Eulerian code. Figure 89.7 shows the velocity profiles ( $v_x$  and  $v_y$ ) at two different times, calculated using results of simulations for the fluid interface with  $A_T = 0.4$  and the initial amplitude of velocity perturbation  $v_0 = 0.01\sqrt{g\lambda}$ , where  $\lambda$  is the perturbation wavelength. The vertical lines show the interface between the heavier and lighter fluids (the heavier fluid is on the right side of the lines). Velocity  $v_y$  is plotted at the position of the bubble center ( $x = 0$ ), and the transverse velocity  $v_x$  is plotted at  $x = 0.02\lambda$  [ $v_x(x = 0) = 0$  at all times]. When the



TC5885

Figure 89.7

Velocity profiles at two different times calculated using results of a 2-D simulation. Dashed lines represent profiles in the linear regime, and solid lines correspond to velocities in the nonlinear regime.

perturbations are in the linear regime ( $k\eta_0 \ll 1$ ), the velocity decays exponentially from the interface toward the lighter and heavier fluids (dashed lines). As the bubble amplitude becomes nonlinear ( $k\eta_0 > 1$ ), the longitudinal velocity  $v_y$  in the light fluid flattens out near the bubble tip and the transverse velocity goes to zero (solid lines), in agreement with the results of Eq. (11).

Applying the model to the Richtmyer–Meshkov (RM) instability, we take the limit of  $g \rightarrow 0$  in Eq. (8). The asymptotic bubble velocity in this case becomes

$$U_{\text{RM}} \rightarrow \frac{3 + A_T}{3(1 + A_T)} \frac{1}{kt}. \quad (12)$$

In his original paper,<sup>4</sup> Layzer takes only the first harmonic as a solution of the Laplace equation (1). Later, several attempts have been made to construct an exact solution for the case of  $A_T = 1$  near the tip of the bubble, writing the solution of Eq. (1) as a Fourier series:<sup>3</sup>

$$\phi = \sum_{l=1}^{\infty} a_l e^{ilkx - lky}. \quad (13)$$

It can be shown,<sup>3</sup> however, that keeping the first two terms in the expansion and applying the boundary conditions up to the fourth order in  $x$  leads to an imaginary component in the solution for the asymptotic bubble velocity. To overcome this difficulty, Refs. 3 have suggested keeping the bubble curvature  $R$  as a free parameter of the problem, limiting the values of  $R$  by the convergence condition of series (13). We propose a different approach to construct an exact solution that is valid near the bubble tip. It can be shown that writing the velocity potential in the form

$$\phi^h = \sum_{l=0}^{\infty} a_{2l+1} \cos[(2l+1)kx] e^{-(2l+1)k(y-\eta_0)}, \quad (14)$$

$$\phi^l = \sum_{l=0}^{\infty} b_{2l+1} \cos[(2l+1)kx] e^{(2l+1)k(y-\eta_0)} + b_2 y \quad (15)$$

leads to a real value of bubble velocity in all approximation orders. Such an expansion requires no additional free parameters to provide convergence for the solution. Figure 89.8 shows plots of the first four coefficients  $a_{1-7}$  as functions of

time for the case of  $A_T = 1$ . Observe that coefficients  $a_l$  decay exponentially with  $l$ , satisfying the convergence condition. Next, we calculate asymptotic values of  $\eta_2$  and  $U_b$  using solution (14)–(15). The result is

$$\eta_2(t \rightarrow \infty) = -\frac{k}{4.88}, \quad U_b(\infty) = 1.025 \sqrt{\frac{2A_T}{1+A_T} \frac{g}{3k}}. \quad (16)$$

The convergence of solution (14)–(15) is very fast. Keeping only two terms in each sum in  $\phi^h$  and  $\phi^l$  gives the solution for  $\eta_2$  and  $U_b$  within 99.5% accuracy. Remarkably, the values given in Eq. (16) are in agreement with the results of Ref. 3 (for  $A_T = 1$ ), where the authors introduced a free parameter  $R$ . This parameter was chosen at the edge point of the region where the Fourier series (13) converges.

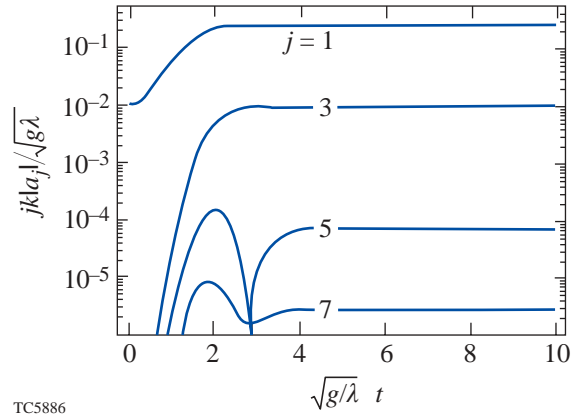


Figure 89.8  
Coefficients  $a_{1-7}$  of the Fourier series (14) for  $A_T = 1$ .

To validate the analysis described above, we compare the results of the model with numerical simulations. Figure 89.9 shows the bubble evolution for the case of  $A_T = 0.1$  and  $A_T = 0.4$ . We start the simulation by imposing a velocity perturbation with amplitude  $v_0 = 0.01\sqrt{g\lambda}$ . Solid lines represent the solution of Eq. (8); solid dots ( $A_T = 0.4$ ) and solid squares ( $A_T = 0.1$ ) correspond to the results of simulations. Good agreement between theory and simulations confirms the accuracy of the model. Next, we comment on a possibility of applying the Layzer-type analysis to study evolution of the spikes. Reference 8 has shown that such an analysis gives quite a reasonable agreement with simulations for the case of  $A_T = 1$ . The appropriate velocity potential for the spikes at  $A_T < 1$  in the Layzer-type model has the form

$$\phi^h = a_1 \cos(kx) e^{-k(y-\eta_0)} + a_2 y,$$

$$\phi^l = b_1 \cos(kx) e^{k(y-\eta_0)}.$$

Substituting the above expressions into Eqs. (2)–(4) and expanding the latter until the second order in  $x$  gives the evolution equations that can be obtained from Eqs. (7) and (8) by substituting  $\eta \rightarrow -\eta$ ,  $A_T \rightarrow -A_T$ , and  $g \rightarrow -g$ . Taking the limit of  $t \rightarrow \infty$ , the asymptotic spike velocity becomes

$$U_s = \sqrt{2A_T/(1-A_T)(g/3k)}.$$

The last formula agrees with the prediction of the drag-buoyancy model.<sup>6</sup> Simulations, however, show that the spike velocity for the interfaces with  $A_T > 0.1$  does not saturate to a constant value. Figure 89.9 shows the spike amplitudes calculated using the simulation (open circles for  $A_T = 0.4$  and open squares for  $A_T = 0.1$ ) and the results of the model (dashed lines). As seen from the results of the simulations, the spike velocity for  $A_T > 0.1$  keeps growing linearly in time, even after perturbations become nonlinear. This is caused by the formation of vortices in the proximity of the spike tip. If the Atwood number is not too small, vortices move with the spike, modifying its velocity field and accelerating the spike into the light fluid. Thus, to describe the spike in the nonlinear regime, the velocity potential must be modified to include evolution of the vortices. This is a subject of current research.

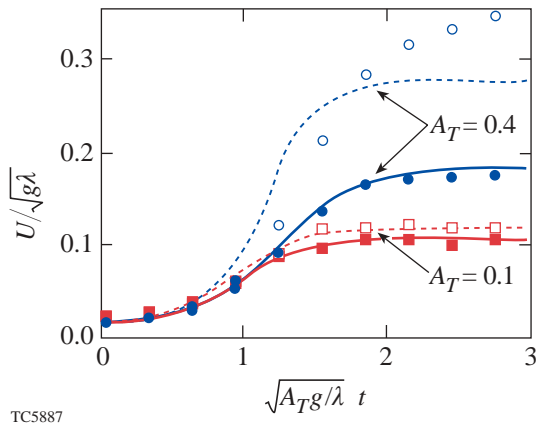


Figure 89.9  
Bubble (solid lines, solid circles and squares) and spike (dashed lines, open circles and squares) velocities calculated using the potential model (lines) and numerical simulation (circles and squares).

The procedure described above for the 2-D flow can be applied to analyze the bubble evolution in 3-D geometry. Taking the  $z$  axis in the direction of the density gradient and assuming cylindrical symmetry of the bubble, the velocity potential in the heavy and light fluids takes the form  $\phi^h = a(t) J_0(kr) e^{-kz}$ ,  $\phi^l = b_1(t) J_0(kr) e^{kz} + b_2(t) z$ , where  $J_0(x)$  is the Bessel function of zero order. Expanding the velocity potential and the jump conditions across the fluid interface up to the second order in  $r$  yields the following system:

$$\eta_2 = -\frac{k}{8} + \left[ \frac{k}{8} + \eta_2(0) \right] e^{-2k[\eta_0 - \eta_0(0)]}, \quad (17)$$

$$\begin{aligned} \ddot{\eta}_0 & \frac{k^2 - 4A_T k \eta_2 - 32A_T \eta_2^2}{4(k - 8\eta_2)} \\ & + \dot{\eta}_0^2 k^2 \frac{(5A_T - 4)k^2 + 16(2A_T - 3)k\eta_2 + 64A_T \eta_2^2}{8(k - 8\eta_2)^2} \\ & + A_T g \eta_2 = 0. \end{aligned} \quad (18)$$

The asymptotic bubble velocity and  $\eta_2$  derived from the system (17)–(18) take the form

$$\eta_2(t \rightarrow \infty) = -k/8,$$

$$U_b^{3-D}(\infty) = \sqrt{2A_T/(1+A_T)(g/k)}.$$

For the RM case ( $g = 0$ ), the asymptotic bubble velocity becomes  $U_{RM}^{3-D} = 2/(1+A_T)/(kt)$ . Repeating calculations by keeping higher harmonics in the expansion

$$\phi^h = \sum_{l=0}^{\infty} a_{2l+1} J_0[(2l+1)kr] e^{-(2l+1)kz},$$

$$\phi^l = \sum_{l=0}^{\infty} b_{2l+1} J_0[(2l+1)kr] e^{(2l+1)kz} + b_2 z,$$

the asymptotic bubble velocity converges to

$$U_b^{3-D} \sim 1.02 \sqrt{\frac{2A_T}{1+A_T} \frac{g}{k}}, \quad \eta_2 \rightarrow -\frac{k}{6.7}. \quad (19)$$

For  $A_T = 1$ , these values are close to the results of Ref. 3, where authors have found the following values:  $U_b = 0.99\sqrt{g/k}$  and  $\eta_2 = -k/6.4$ .

In summary, the nonlinear analytical model of the classical single-mode RT instability at arbitrary Atwood numbers was developed. The model gives a continuous bubble evolution from the exponential growth to the nonlinear regime, where the bubble velocity saturates at

$$U_b^{2-D} = \sqrt{2A_T/(1+A_T)(g/3k)}$$

and

$$U_b^{3-D} = \sqrt{2A_T/(1+A_T)(g/k)}.$$

The results of the model agree very well with the numerical simulations and predictions of the drag–buoyancy model.<sup>6</sup>

#### ACKNOWLEDGMENT

The author thanks Prof. Dov Shvarts and his group, Prof. R. Betti, Prof. J. Sanz, and Dr. C. Cherfils-Cl  rouin for many helpful discussions. This work was supported by the U.S. Department of Energy Office of Inertial Confinement Fusion under Cooperative Agreement No. DE-FC03-92SF19460, the University of Rochester, and the New York State Energy Research and Development Authority. The support of DOE does not constitute an endorsement by DOE of the views expressed in this article.

#### REFERENCES

1. Lord Rayleigh, in *Scientific Papers* (Cambridge University Press, Cambridge, England, 1900), Vol. II.
2. B. A. Remington *et al.*, *Phys. Plasmas* **7**, 1641 (2000); J. D. Lindl, *Inertial Confinement Fusion: The Quest for Ignition and Energy Gain Using Indirect Drive* (Springer-Verlag, New York, 1998).
3. N. A. Inogamov and S. I. Abarzhi, *Physica D* **87**, 339 (1995); S. I. Abarzhi, *Phys. Rev. E* **59**, 1729 (1999).
4. D. Layzer, *Astrophys. J.* **122**, 1 (1955).
5. G. B. Whitham, *Linear and Nonlinear Waves*, Pure and Applied Mathematics (Wiley, New York, 1974), p. 473; J. W. Jacobs and I. Catton, *J. Fluid Mech.* **187**, 329 (1988); M. J. Dunning and S. W. Haan, *Phys. Plasmas* **2**, 1669 (1995).
6. D. Oron *et al.*, *Phys. Plasmas* **8**, 2883 (2001); U. Alon *et al.*, *Phys. Rev. Lett.* **74**, 534 (1995); G. Dimonte, *Phys. Plasmas* **7**, 2255 (2000); G. Dimonte and M. Schneider, *Phys. Fluids* **12**, 304 (2000).
7. K. O. Mikaelian, *Phys. Rev. Lett.* **80**, 508 (1998).
8. Q. Zhang, *Phys. Rev. Lett.* **81**, 3391 (1998).
9. S. Wolfram, *The Mathematica Book*, 3rd ed. (Wolfram Media/Cambridge University Press, 1996).